The GERDA Experiment and the Search for Neutrinoless Double Beta Decay

Björn Lehnert on behalf of the GERDA Collaboration
Institut für Kern- und Teilchenphysik, Technische Universität Dresden, Dresden, Germany

The GERDA experiment (GERmanium Detector Array) investigates the neutrinoless double beta decay in ^{76}Ge and is among the leading experiments in the field. The experiment is planned in two phases; the data taking of Phase I ended last summer after 21.6 kg·yr exposure with a background level of $1{\cdot}10^{-2}$ cts/(kg · yr · keV) after pulse shape discrimination. A lower half-life limit of $T^{0\nu}_{1/2} > 2.1{\cdot}10^{25}$ yr (90 % C.L.) was established. The transition to Phase II with major upgrades and additional target mass is currently ongoing. The goal for Phase II is a background level of 10^{-3} cts/(kg · yr · keV). With an exposure of 100 kg · yr a sensitivity for a lower half-life limit of $1.4{\cdot}10^{26}$ yr can be reached. This paper will introduce the GERDA experiment with a focus on the recent results of Phase I data along with their implications with respect to the controversial claim of $0\nu\beta\beta$ observation by a subgroup of the Heidelberg-Moscow experiment.

1 Introduction

Double beta decay is a second order weak nuclear decay that can occur in specific configurations where two consecutive single beta decays are energetically forbidden or otherwise strongly suppressed. There are 35 candidate isotopes for double beta minus decay. The two neutrino double beta decay ($2\nu\beta\beta$) is a Standard Model process and has been observed in 11 of these isotopes [1,2]. The final state particles of the $2\nu\beta\beta$ are two neutrinos and two electrons sharing the decay energy. The experimental signature is the sum of the electron energies in a continuous spectrum.

The existence of neutrinoless double beta decay ($0\nu\beta\beta$) is well motivated by many theories beyond the Standard Model [3]. The absence of neutrinos in the final state violates lepton number by two units and is a powerful tool in the search for new physics. The lepton number violation (LNV) can be generated by many proposed processes but is easiest motivated by the "standard interpretation" with light Majorana neutrinos. The rate $\Gamma^{0\nu}$ or half-life $T^{0\nu}_{1/2}$ of the decay is connected with strength of the LNV parameter $\langle\eta\rangle$ by

$$\left(T^{0\nu}_{1/2}\right)^{-1} = \frac{\Gamma^{0\nu}}{\ln(2)} = G^{0\nu}(Q_{\beta\beta}, Z) \cdot \left|M^{0\nu}\right|^2 \cdot \langle\eta\rangle^2 \qquad (1)$$

requiring a nuclear matrix element $M^{0\nu}$ and a phase space factor $G^{0\nu}(Q_{\beta\beta}, Z)$. In the case of light Majorana neutrinos exchange, $\langle\eta\rangle$ is the Majorana neutrino mass $|m_{ee}|$ defined as the coherent sum of the electron neutrino mass eigenstates:

$$|m_{ee}| = \left| m_1|U_{e1}|^2 + m_2|U_{e2}|^2 e^{i(\alpha_2-\alpha_1)} + m_3|U_{e3}|^2 e^{-i(\alpha_1+2\delta)} \right|. \quad (2)$$

The virtual nature of this neutrino propagator makes this mass definition dependent on the CP phase δ and the two Majorana phases α_1 and α_2. Thus, $0\nu\beta\beta$ can probe the Majorana nature of neutrinos, the Majorana phases and the absolute neutrino mass scale assuming the standard interpretation of $0\nu\beta\beta$. The experimental signature is that the two final state electrons carry the available decay energy. A peak is expected in the energy spectrum at the Q-value at e.g. 2039 keV for ^{76}Ge. The observation of this peak implies LNV independent of a model.

The nuclear matrix elements (NME) are calculated using theoretical nuclear models and have different values for the various double beta decay isotopes. Large differences persist between different theoretical approaches introducing uncertainties for the inference of the Majorana neutrino mass and the conversion between half-life measurements of different isotopes.

The observation of 28.8 ± 6.9 $0\nu\beta\beta$ events in ^{76}Ge has been reported by a subset of the Heidelberg Moscow collaboration in 2004. They claim a half-life of $T^{0\nu}_{1/2} = 1.19^{+0.37}_{-0.23} \cdot 10^{25}$ yr [4]. This claim has been further investigated with a pulse shape analysis in 2006 [5]; however, the latter publication shows internal inconsistencies [6] and is not considered for comparison by GERDA.

Today, there are a variety of neutrinoless double beta decay experiments investigation different candidate isotopes. They are utilizing various detection techniques optimizing a large target mass with a good energy resolution. Apart from the GERDA result, recently published limits for $0\nu\beta\beta$ are from Kamland-Zen [17] and EXO-200 [19] reaching lower half-live limits for ^{136}Xe of $1.9 \cdot 10^{25}$ yr and $1.1 \cdot 10^{25}$ yr (90 % C.L.) respectively.

2 The GERDA Experiment

The GERDA experiment is designed in two physics phases: Phase I was planed to demonstrate the operation of HPGe detectors inside liquid argon (LAr) and to directly test the claim in ^{76}Ge in a model independent way. The data taking started in November 2011 and finished in May 2013. Phase II is planed to start in 2014 and increases the sensitivity to half-lives around $1.4 \cdot 10^{26}$ yr.

GERDA is designed with the concept of operating an array of bare HPGe detectors directly in a cryogenic liquid as suggested in [7]. This approach combines the advantages of a radio pure passive shielding and a scintillation based active shielding while providing the cryogenic cooling for the operation of the detectors.

The general setup is described in [8] and illustrated in Figure 1. The outer vessel is a 590 m^3 stainless steel water tank instrumented with 66 PMTs and VM2000 reflective foil serving as a Cherenkov muon veto and a passive shield from outside radiation. The underground location at the Laboratori Nazionali del Gran Sasso (LNGS) provides an overburden of 3500 m w.e. and reduces the cosmic muon flux by a factor of 10^6. The residual muons with a flux of 1.2 (h·m^2)$^{-1}$ are tagged by the muon veto with more than 99.9 % efficiency. The inner vessel is a double-walled stainless steel cryostat containing 64 m^3 of grade 5 LAr.

The array of HPGe detectors is segmented in strings of 3 to 5 detectors and supported by low mass Cu holders. The detector strings are lowered down into the cryostat from a clean room on top of the superstructure. The clean room contains a glove box for detector operations in nitrogen atmosphere and a two-arm lock system supporting one string on one arm and a combination of three strings on another. For Phase I, eight enriched and one non-enriched semi-coaxial detectors were deployed in the three-string arm. The one-string arm was equipped with two non-enriched semi-coaxial detectors until July 2012 and then with five enriched Broad Energy

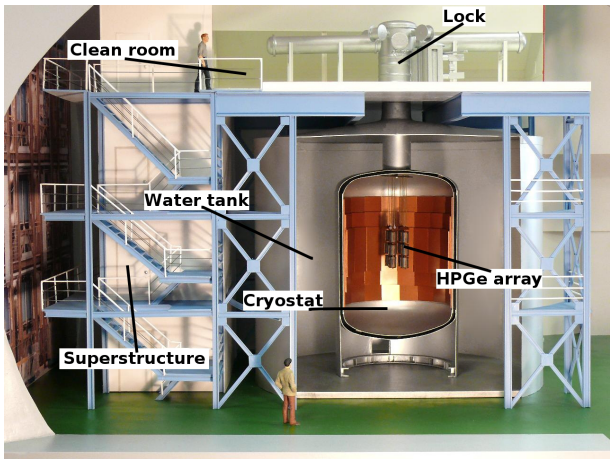

Figure 1: Illustration of the GERDA setup [8]. Germanium detector array not to scale.

Germanium (BEGe) detectors. Five of the enriched semi-coaxial detectors were refurbished from the Heidelberg-Moscow (HdM) experiment and three from the International Germanium experiment (IGEX). The non-enriched semi-coaxial detectors were refurbished form the GENIUS Test Facility (GTF). The enriched BEGe detectors are costum made for the GERDA experiment.

The front-end electronics consist of custom made charge sensitive preamplifiers placed at $\approx 30\,\mathrm{cm}$ distance to the top of the detector strings inside the LAr. The charge signal is sampled with a 100 MHz FADC. A window of $160\,\mu\mathrm{s}$ is recorded in case of a trigger from any detector in the array. The trigger threshold is equivalent of 40 - 100 keV. The raw DAQ output is transformed into ROOT format [11] and propagated through a multi-tier analysis chain [12]. A blinding procedure is applied on the raw data conversion; events in the energy window $Q_{\beta\beta}\pm 20\,\mathrm{keV}$ are not processed and remain hidden during the analysis.

3 Phase I analysis

For the $0\nu\beta\beta$ analysis [13] the total Phase I data is used and separated between BEGe and semi-coaxial detectors due to their different properties. The semi-coaxial data set is further divided into a *golden* and *silver* data set due to a short increase in the background level at the time of detector operation in July 2012 for the BEGe insertion. The three data sets amount to a total live-time of 492.3 d and $21.6\,\mathrm{kg\cdot yr}$ of enriched germanium. A summary of the data sets is shown in Table 1.

The energy scale is monitored with weekly ^{228}Th calibrations; the energy shift between consecutive calibrations is smaller than 1 keV at $Q_{\beta\beta}$. The deviation of reconstructed peak positions from the calibration curves is smaller than 0.3 keV. The calibrations are also used to monitor the energy resolution which was stable over the time of the Phase I data taking. A comparison of the energy resolution of the 1524.6 keV ^{42}K γ-line in the background spectrum shows a FWHM of 4.5 keV compared to 4.3 keV as expected from the calibration curves; this small variation illustrates the good stability of the energy scale between calibrations. The exposure-averaged energy resolutions are 4.8 ± 0.2 keV and 3.2 ± 0.2 keV FWHM at $Q_{\beta\beta}$ for the semi-coaxial detectors and the BEGe detectors, respectively.

The spectrum of a subset of the Phase I data is shown in Figure 2 (left) for the enriched semi-coaxial and BEGe detectors. The dominating features are from ^{39}Ar at low energies, the $2\nu\beta\beta$ of ^{76}Ge and the 1524.6 keV ^{42}K γ-line at intermediate energies and α-structures at high energies. Additionally, γ-lines from ^{40}K, ^{214}Bi, ^{214}Pb and the ^{228}Th decay chain can be identified.

^{39}Ar is a pure beta emitter with an endpoint of 565 keV. Although dominating the total count rate, it has no influence on the $0\nu\beta\beta$ ROI. The spectrum above 600 keV is decomposed into the before mentioned contributions with a background model reported in [9]. Above 600 keV,

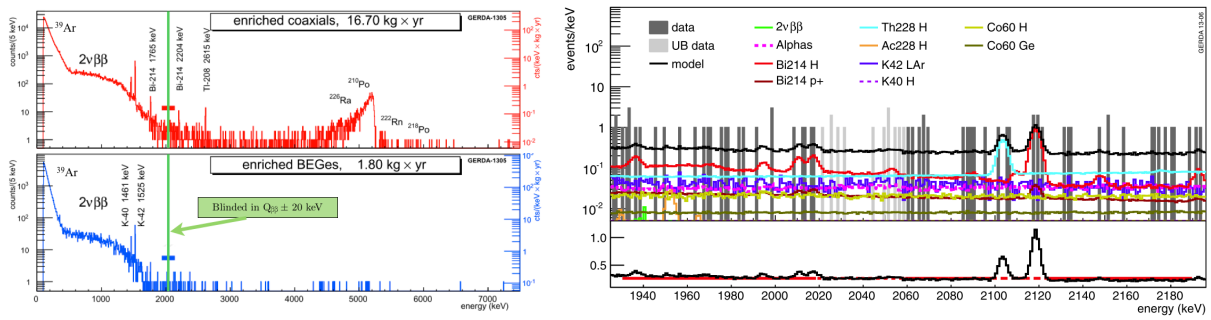

Figure 2: Spectra of Phase I background data. Left: Full energy range devided into semi-coaxial data (top) and BEGe data (bottom) [9]. Right: Zoom of ROI with background model overlaid [9]. Here events $Q_{\beta\beta}\pm5$ keV are not shown.

the ^{76}Ge $2\nu\beta\beta$ component is clearly visible. A dedicated analysis for $2\nu\beta\beta$ was performed with 5.04 kg · yr of Phase I data and is reported in [10]. The analysis yields a $2\nu\beta\beta$ half-life of $T^{2\nu}_{1/2} = \left[1.84^{+0.09}_{-0.08}\,(\text{fit})\,^{+0.11}_{-0.06}\,(\text{syst})\right] \cdot 10^{21}$ yr with a non preceded signal-to-background ratio of 4:1 for this process in ^{76}Ge. The most prominent γ-line originates from ^{42}K which is part of a decay chain starting from ^{42}Ar present in natural argon. ^{42}K has a Q-value of 3525.4 keV and beta-decays with 81.9 % probability into the ground state. The decay branch with the 1524.6 keV γ-line has 17.6 % probability. Especially for decays into the ground state, the resulting high energy β's have the potential to penetrate the n^+ dead layers of germanium detectors which are in the range of 2 mm for the semi-coaxial detectors and 0.8 mm for the BEGe detectors. For the thin dead layer BEGe detectors, more than 50 % of the background in the ROI is attributed to ^{42}K surface event.

The events at higher energy originate from α decays on the p^+ contact surface which has a dead layer thickness of a few μm. The p^+ contact area is larger in the semi-coaxial detectors including the detector bore hole and thus making this detector type more prone to α contributions. See also the spectral difference in Figure 2 (left). The main α component is identified as ^{210}Po. The contribution of the α background in the ROI is estimated between 10 to 15 % for semi-coaxial detectors. The major background contributions at $Q_{\beta\beta}$ are identified as ^{214}Bi and ^{208}Tl in the detector holders. The background contributions around $Q_{\beta\beta}$ are shown in Figure 2 (right) for the semi-coaxial data. The ultimate conclusion from the background decomposition is the validation of a flat continuous background assumption in the energy window of ≈ 200 keV around $Q_{\beta\beta}$ and the absence of known peaks in the ROI.

The event topology of $0\nu\beta\beta$ are two electrons that deposit their energy almost always inside a small volume inside a single detector. Events with energy depositions in more than one detector and events within a muon veto trigger window of 8 μs are removed from the data set. This removes roughly 40 % of events around $Q_{\beta\beta}$. A coincidence veto within 1 ms, designed to reject ^{214}Bi - ^{214}Po events, removes two events. These cuts practically do not reduced the detection efficiency for $0\nu\beta\beta$ nor introduce a dead time.

A pulse shape discrimination (PSD) cut is applied to discriminate surface and gamma background in the surviving event sample [14]. Gamma interactions around $Q_{\beta\beta}$ predominantly scatter inside one detector and produce multi-site events that can be identified in the waveforms of the recorded charge traces. Surface events such as β or α events pass the n^+ or p^+ surfaces and can be discriminated from bulk events. The charge signal results in a slower or faster risetime for the n^+ or p^+ surface respectively.

The PSD method for the BEGe detectors is the ratio A/E of the current pulse amplitude (A) and the reconstructed energy (E). For a $0\nu\beta\beta$ survival efficiency of 0.92 ± 0.02 more than 80 % of the counts in the BI window are removed. The pulse shape analysis for semi-coaxial detectors is significantly less effective due to a larger variety of pulse shapes for $0\nu\beta\beta$-like events.

Table 1: Summary of Phase I data sets for $0\nu\beta\beta$ analysis.

Data set	exposure [kg·yr]	background level [10^{-2} cts /(keV·kg·yr]		expected counts $Q_{\beta\beta}\pm5$ keV		observed counts $Q_{\beta\beta}\pm5$ keV	
		w PSD	w/o PSD	w PSD	w/o PSD	w PSD	w/o PSD
Golden	17.9	1.8 ± 0.2	1.1 ± 0.2	3.3	2.0	5	2
Silver	1.3	$6.3^{+1.6}_{-1.4}$	$3.0^{+1.1}_{-0.9}$	0.8	0.4	1	1
BEGe	2.4	$4.2^{+1.0}_{-0.8}$	$0.5^{+0.4}_{-0.3}$	1.0	0.1	1	0
Sum	21.6			5.1	2.5	7	3

A TMlpANN neutral network is used to separate single and multi-site events. With a fixed single-site survival efficiency of 0.90, about 45 % of counts in the BI window are remove. The performances are cross checked with two independent methods and with $2\nu\beta\beta$ events [14].

The unblinding of the $Q_{\beta\beta}\pm20$ keV window was performed in two steps: In a first step the 15 keV wings of the window were unblinded to cross check the understanding of the background. Then, the data set, all cuts and the statistical analysis were fixed prior to the second step: the processing of the events inside remaining window of $Q_{\beta\beta}\pm5$ keV.

4 Results on $0\nu\beta\beta$

After the processing of the events in $Q_{\beta\beta}\pm5$ keV, 7 events were found before PSD and 3 events after PSD. This can be compared to 5.1 and 2.5 expected background events respectively. The observed number of counts in the ROI is consistent with the background expectation and no signal is found. See also Table 1 for the results of the individual data sets.

A profile likelihood fit is used to extract a lower half-life limit. The fit function is a gaussian peak with a constant background. It is used on each data set with $1/T^{0\nu}_{1/2}$ as a common parameter. The width of the gaussian is fixed to the known energy resolution of each data set. The mean is centered around $Q_{\beta\beta}\pm0.2$ keV. The background is left unconstrained for each set in a 240 keV window from 1930 keV to 2190 keV. Excluded are ±5 keV windows around known γ-lines of 2104 keV from ^{208}Tl and 2119 keV from ^{214}Bi.

The signal strength is not allowed to be negative: $1/T^{0\nu}_{1/2} \geq 0$. Systematic uncertainties (such as the peak position, the resolution and all efficiencies) are folded into the analysis a posteriori by Monte Carlo: The result is the average limit of 10000 simulated experiments with randomly generated sets of parameters in the allowed space of the systematic uncertainties. The best fit yields 0 counts and the 90% quantile yields a lower half-life limit of

$$T^{0\nu}_{1/2} \geq 2.1 \cdot 10^{25}\,\text{yr} \quad (90\,\%\ \text{C.L.}).$$

Without systematic errors the limit improves by 1.5 %. The sensitivity, defined as the median value of a set of 10000 toy Monte Carlo experiments with the background only assumption, is $T^{0\nu}_{1/2} \geq 2.4 \cdot 10^{25}$ yr (90 % C.L.).

The results from the IGEX [15] and HdM [16] experiments can be included in this analysis as a 4th and a 5th data set. A combined lower half-life limit for ^{76}Ge is set to:

$$T^{0\nu}_{1/2} \geq 3.0 \cdot 10^{25}\,\text{yr} \quad (90\,\%\ \text{C.L.}).$$

The 2004 claim [4] is tested with the GERDA data. Two hypotheses are compared: The H_1 hypothesis with a $0\nu\beta\beta$ half-life of $1.19^{+0.37}_{-0.23}\cdot10^{25}$ yr and the H_0 hypothesis with the background only assumption. 5.9 signal and 2.0 background events are expected in $Q_{\beta\beta}\pm2\sigma_E$ for H_1 in the GERDA data set after PSD. Three events are observed and the spectral fit yields 0 signal

events. The probability to observe no event assuming H_1 is $p(\text{data}|H_1) = 0.01$; hence the claim is strongly disfavored. The Bayes factor defined as $B = p(\text{data}|H_1)/p(\text{data}|H_0)$ is $B = 0.024$. The combined result for ^{76}Ge yields $B = 2 \cdot 10^{-4}$.

The results from ^{76}Ge can be compared with the ^{136}Xe results from Kamland-ZEN [17] and EXO [18,19] via the two NME values for each isotopes. This is illustrated in Figure 3. The half-lives for ^{136}Xe and ^{76}Ge are shown on the x and y axis, respectively. The conversion is performed via the lines for different NME calculations. The half-life values for 0.2, 0.3 and 0.4 eV effective Majorana neutrino mass are shown as blue, magenta and red markers respectively. The claim [4] is shown as a green band. The combined ^{136}Xe half-live is excluding the claim with $> 97.5\,\%$ C.L. even for the most unfavorable NME calculation [17]. However, the shown conversion from a ^{136}Xe to a ^{76}Ge half-life is assuming dominant light Majorana neutrino exchange and only ^{76}Ge based experiment can test the claim in a model independent way.

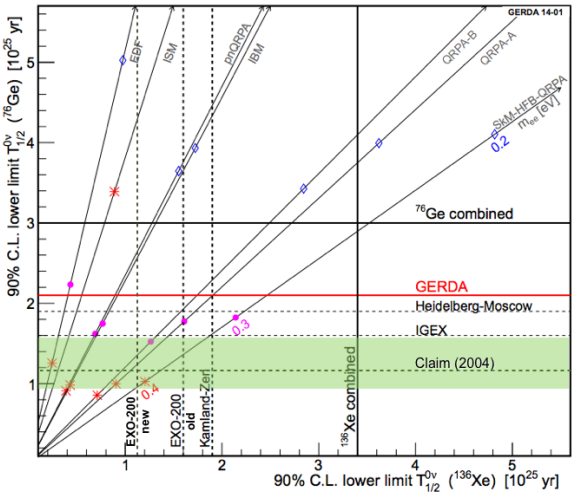

Figure 3: Comparison of recent results in ^{136}Xe [17,18,19] and ^{76}Ge [13]. The diagonal lines show half-life conversions for various NME calculations: EDF [20], ISM [21], IBM [22], pnQRPA [23], QRPA [24] and SkM-HFB-QRPA [25]. The markers denote the calculated half-lives for a Majorana neutrino mass of 0.2, 0.3 and 0.4 eV in blue, magenta and red respectively. The green band shows the 2004 claim [4] with 68 % C.L. error band.

5 Conclusion and Outlook

A blind analysis for $0\nu\beta\beta$ was performed on the GERDA Phase I data set. An exposure of 21.6 kg·yr with a background level of 0.01 cts /(keV·kg·yr) was reached after pulse shape. No signal is observed and a new best lower half-life limit is set to $2.1 \cdot 10^{25}$ yr (90 % C.L.). The previous claim of $0\nu\beta\beta$ is compatible with GERDA data only with 1 % probability. The scrutinization of the claim is done in a model independent way using partly the same germanium detectors.

Phase II of the GERDA experiment will start in 2014 and use 30 additional BEGe detectors which increase the target mass by 20 kg of enriched material. The background level is aimed to be lowered to 0.001 cts /(keV·kg·yr) with improved PSD performance of BEGe detectors and a LAr scintillation light read out. The expected half-life sensitivity is $1.4{\cdot}10^{26}$ yr after 100 kg·yr translating into a sensitivity for the Majorana neutrino mass of 100 meV depending on the NME.

References

1. V. I. Tretyak and Y. G. Zdesenko, At. Data Nucl. Data Tables 80, 83 (2002).
2. N. Ackerman et al. (EXO Collaboration), Phys. Rev. Lett. 107, 212501 (2011).

3. W. Rodejohann, Int. J. Mod. Phys. E 20, 1833 (2011).
4. H. V. Klapdor-Kleingrothaus et al., Phys. Lett. B 586, 198 (2004).
5. H. V. Klapdor-Kleingrothaus and I. Krivosheina, Mod. Phys. Lett. A 21, 1547 (2006).
6. B. Schwingenheuer, Ann. Phys. 525, 269 (2013).
7. G. Heusser, Annu. Rev. Nucl. Part. Sci. 45, 543 (1995).
8. K.-H. Ackermann et al. (GERDA Collaboration), Eur. Phys. J. C 73, 2330 (2013).
9. M. Agostini et al. (GERDA Collaboration), Eur. Phys. J. C 74, 2764 (2014).
10. M. Agostini et al. (GERDA Collaboration), J. Phys. G 40, 035110 (2013).
11. R. Brun, F. Rademakers, NIM A 389,81 (1997).
12. M. Agostini, L. Pandola, P. Zavarise, O. Volynets, J. Instrum. 6, P08013 (2011).
13. M. Agostini et al. (GERDA Collaboration), Phys. Rev. Lett. 111, 122503 (2013).
14. M. Agostini et al. (GERDA Collaboration), Eur. Phys. J. 73, 2583 (2013).
15. C. E. Aalseth, et al., Phys. Rev. D 65, 092007 (2002).
16. H. V. Klapdor-Kleingrothaus, et al., Eur. Phys. J. A 12, 147 (2001).
17. A. Gando et al. (Kamland-ZEN Collaboration), Phys. Rev. Lett. 110, 062502 (2013).
18. M. Auger et al. (EXO Collaboration), Phys. Rev. Lett. 109, 032505 (2012).
19. J.B. Albert et al. (EXO Collaboration), arXiv:1402.6956 [nucl-ex] (2014).
20. T. R. Rodriguez and G. Martinez-Pinedo, Phys. Rev. Lett. 105, 252503 (2010).
21. J. Menendez et al., Nucl. Phys. A 818, 139 (2009).
22. J. Barea, J. Kotila and F. Iachello, Phys. Rev. C 87, 014315 (2013).
23. J. Suhonen and O. Civitarese, Nucl. Phys. A 847, 207 (2010).
24. F. Simkovic, V. Rodin, A. Faessler and P. Vogel, Phys. Rev. C. 87, 045501 (2013).
25. M. T. Mustonen and J. Engel, arXiv:1301.6997 (2013).